VNU Journal of Science: Mathematics – Physics, Vol. 40, No. 1 (2024) 83-95

VNU Journal of Science: Mathematics - Physics

Journal homepage: https://js.vnu.edu.vn/MaP

Original Article

Nonlinear Vibration of Saturated Porous Functionally Graded Plate in Thermal Environment

Tran Quoc Quan*, Nguyen Dang Hung, Vu Duc Thang

VNU University of Engineering and Technology, 144 Xuan Thuy, Cau Giay, Hanoi, Vietnam

Received 10 October 2023
Revised 23 October 2023; Accepted 18 March 2024

Abstract: In this work we studied investigates the nonlinear vibrations of a rectangular saturated porous functionally graded (FG) plate on elastic foundations in thermal environment. The mechanical properties of the saturated porous material vary smoothly with the thickness in three different distributions of porosity including uniform, symmetrically irregular, and asymmetrically irregular. The basic equations are employed by the Reddy's higher order shear deformation theory, incorporating the geometrically nonlinear von Kármán strain-displacement relationship, stress-strain relations based on the elastic theory for porous materials by Biot, and an analytical solution obtained through the Galerkin method and Airy's stress function for the simply supported plate. The influence of the geometrical and material parameters, elastic foundations and temperature increment on the nonlinear vibrations of the saturated porous FG plate were specifically evaluated through numerical investigations.

Keywords: Vibration; saturated porous plate; thermal environment; elastic foundations; Biot theory.

1. Introduction

Porous functionally graded materials with cellular structures are among the advanced types of advanced composite materials. Possessing excellent energy absorption capabilities, lightweight properties, low thermal and electrical conductivity coefficients, along with several other distinctive features, porous materials have potential applications in creating energy and sound absorption systems, porous electrodes, electromagnetic shielding, and medicine. Static and dynamic analyses of beam, plate, and shell structures made of porous materials under the influence of various loads consistently attract the interest of the research community. Xue et al., [1] investigated the free vibration behaviors of

* Corresponding author.
E-mail address: quantq@vnu.edu.vn

https//doi.org/10.25073/2588-1124/vnumap.4884

functionally graded porous cylindrical panels and shells by utilizing the first order shear deformation theory in conjunction with Hamilton's principle. Chaabani et al., [2] presented an effective approach to investigating the buckling and post-buckling behavior of porous FGM plates using higher order shear deformation theory. Further, He et al., [3] delved into the nonlinear vibration characteristics and response of a doubly curved shallow shell made of laminated carbon fiber reinforced resin, which had a porous microcapsule coating. This investigation was conducted within a hygrothermal environment and was grounded in the principles of the first-order shear deformation theory; Yang et al., [4] investigated the mechanical properties of FG-GNPRC annular plates with voids in hot and humid environments applying the Newmark method. Recently, Do et al., [5] enhanced the mixed interpolation of tensorial components in triangular elements by employing the edge-based smoothed finite element method to analyze the vibrations of piezoelectric functionally graded porous plates under dynamic loads.

In practice, functionally graded porous structures often exist in a saturated state, where solid-liquid interactions must be considered, and this significantly affects the mechanical behaviors of the structures. When dealing with porous materials, aside from the primary design factors such as the distribution of porosity types and the porosity coefficient, the nature of the fluid within the pores is characterized by the Biot modulus. The Biot modulus is defined as the ratio of the average local pressure within the porosity to the overall pressure acting on the entire structure. Biot's linear elastic theory for saturated porous materials relies on two fundamental assumptions: i) An increase in internal pressure leads to the expansion of porosity, and ii) Compressing the porosity results in elevated pressure within these pores. This theory is frequently applied to investigate the bending, vibration, and stability characteristics of beam and plate structures constructed from saturated porous materials. Civalek et al., [6] examined the nonlinear stability characteristics of saturated porous nanobeams incorporated within an elastic foundation. The restrained nanobeam was represented using geometrical nonlinear equations along with the constitutive law of saturation. Yuan et al., [7] presented a new formulation of smoothed particle finite element method for dynamic problems in two phase saturated porous media. In a work of Zhao et al. [8], the authors developed a mathematical model for the one-dimensional transient response of single-layer saturated porous media, incorporating general boundary conditions, arbitrary initial conditions, and arbitrary vertical loads. This model was based on Biot's fundamental equations for wave propagation in saturated porous media. Besides, Babaei et al., [9] focused on the dynamic behavior of functionally graded saturated porous rotating thick truncated cone using the Biot poroelastic law. Ba et al., [10] introduced a dynamic stiffness matrix approach to study the dynamic response of a multi-scale layered saturated porous half-space caused by a seismic dislocation source, in accordance with Biot's theory of wave propagation in fluid-saturated porous solids.

This paper investigates the nonlinear vibration of saturated porous functionally graded plate subjected to the combination of mechanical and thermal loadings. Three different distributions of porosity are considered. Based on the Biot and higher order shear deformation theories, the vibration characteristics including natural frequency, deflection amplitude – time curves and relation between frequency ratio and amplitude of the saturated porous plate are determined.

2. Modelling of Saturated Porous FG Plate

Consider a rectangular saturated porous plate with dimensions as follows: thickness h, length a, and width b, as depicted in Fig. 1. We assume that the plate rests on elastic foundations characterized by Winkler coefficients k_1 and Pasternak coefficients k_2. The $Oxyz$ Cartesian system, including the xy plane coincides with the central surface, and origin O is located at the corners of the plate.

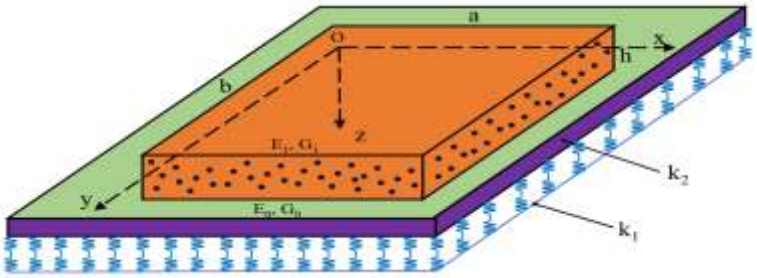

Figure 1. Schematic representation of the saturated porous functionally graded plate on elastic foundations.

The material properties of saturated porous materials vary continuously with the thickness of the plate in three different distributions of porosity as [8-10]

$$\text{Monotonous distribution: } [E,G]=[E_0,G_0](1-e_0\chi),\quad \chi=\frac{1}{e_0}-\frac{1}{e_0}\left(\frac{2}{\pi}\sqrt{1-e_0}-\frac{2}{\pi}+1\right)^2, \tag{1}$$

$$\text{Symmetric distribution: } [E,G]=[E_0,G_0]\left[1-e_0\cos\left(\frac{\pi z}{h}\right)\right], \tag{2}$$

$$\text{Nonsymmetric distribution: } [E,G]=[E_0,G_0]\left[1-e_0\cos\left(\frac{\pi z}{2h}+\frac{\pi}{4}\right)\right], \tag{3}$$

$$e_0=1-E_1/E_0=1-G_1/G_0$$

in which e_0 is the porosity coefficient, E_1, G_1 and E_0, G_0 are Young's modulus and shear modulus at $z=-h/2$ and $z=h/2$, respectively.

3. Basic Equations

The strain field at the mid-plane of the saturated porous functionally graded plate using Reddy's higher order shear deformation theory are expressed as [12]

$$\varepsilon_x^0=\frac{\partial u}{\partial x}+\frac{1}{2}\left(\frac{\partial w}{\partial x}\right)^2,\ \varepsilon_y^0=\frac{\partial v}{\partial y}+\frac{1}{2}\left(\frac{\partial w}{\partial y}\right)^2,\ \gamma_{xy}^0=\frac{\partial u}{\partial y}+\frac{\partial v}{\partial x}+\frac{\partial w}{\partial x}\frac{\partial w}{\partial y},\ \gamma_{xz}^0=\frac{\partial w}{\partial x}+\phi_x,\ \gamma_{yz}^0=\frac{\partial w}{\partial y}+\phi_y \tag{4}$$

where u,v,w are the displacement components of a point on the mid-plane in the x, y, and z directions, respectively. ϕ_x, ϕ_y are the rotation angles of the normal vector of the mid-plane around the y and x axes, respectively.

The strain components at the mid-plane within a distance of z are determined as

$$\begin{aligned}&\varepsilon_x=\varepsilon_x^0+z\phi_{x,x}-c_1z^3\left(\phi_{x,x}+w_{,xx}\right),\ \varepsilon_x=\varepsilon_y^0+z\phi_{y,y}-c_1z^3\left(\phi_{y,y}+w_{,yy}\right),\ \gamma_{xy}=\gamma_{xy}^0\\&+z\left(\phi_{x,y}+\phi_{y,x}\right)-c_1z^3\left(\phi_{x,y}+\phi_{y,x}+2w_{,xy}\right),\ \gamma_{xz}=\gamma_{xz}^0-3c_1z^2\left(w_{,x}+\phi_x\right),\ \gamma_{yz}=\gamma_{xz}^0-3c_1z^2\left(w_{,y}+\phi_y\right)\end{aligned} \tag{5}$$

For saturated porous materials, the stress-strain relationship follows linear elastic theory of Biot as [13]

$$\sigma_{ij}=2G\varepsilon_{ij}+\lambda_u\theta\delta_{ij}-p\alpha\delta_{ij}-3K_u\beta_s\Delta T\delta_{ij},\ i,j=1,2,3 \tag{6}$$

where $\theta=\varepsilon_x+\varepsilon_y+\varepsilon_z$ is the volumetric strain, ΔT is the temperature change from the initial temperature, β_s is the thermal expansion coefficient of the original material under constant pore

pressure; α is the Biot coefficient of effective stress, p is the pore fluid pressure; λ_u the Lamé parameter. These coefficients are determined by

$$p = M\left[\xi - \alpha\theta + \alpha\left(\beta_f - \beta_s\right)T\right],\ \alpha = 1 - \frac{G}{G_1}, M = \frac{2G\left(\nu_u - \nu\right)}{\alpha^2\left(1-2\nu_u\right)\left(1-2\nu\right)}, K_u = \frac{2G\left(1+\nu_u\right)}{3\left(1-2\nu_u\right)},$$
$$\lambda_u = \frac{2G\nu_u}{1-2\nu_u}, \nu_u = \frac{\nu + \alpha B\left(1-2\nu\right)/3}{1-\alpha B\left(1-2\nu\right)/3}, \beta_s = \beta_0\left(1-\alpha\right) \tag{7}$$

with ξ is the variation of fluid volume content, M is Biot's modulus defined as the increase of the amount of fluid, $\nu < \nu_u < 0.5$ is undrained Poisson's ratio, $0 < B < 1$ is the Skempton coefficient reflecting the compressibility of the fluid, β_f is the thermal expansion coefficient of the liquid phase within the pore, β_0 is the thermal expansion coefficient of the homogeneous plate material.

For saturated water plate ($\xi = 0$) and a plane stress problem ($\sigma_z = 0$), Eq. (6) can be rewritten in matrix form as

$$\begin{Bmatrix}\sigma_x\\ \sigma_y\\ \sigma_{xy}\end{Bmatrix} = \begin{bmatrix}Q_{11} & Q_{12} & 0\\ Q_{21} & Q_{22} & 0\\ 0 & 0 & Q_{66}\end{bmatrix}\begin{Bmatrix}\varepsilon_x\\ \varepsilon_y\\ \gamma_{xy}\end{Bmatrix} - c_0 T\begin{Bmatrix}1\\ 1\\ 0\end{Bmatrix};\ \begin{Bmatrix}\sigma_{xz}\\ \sigma_{yz}\end{Bmatrix} = \begin{bmatrix}Q_{55} & 0\\ 0 & Q_{44}\end{bmatrix}\begin{Bmatrix}\gamma_{xz}\\ \gamma_{yz}\end{Bmatrix} \tag{8}$$

with

$$Q_{11} = Q_{22} = 2G(z)\left[1 + \frac{\lambda_u + M\alpha^2}{2G(z) + \lambda_u + M\alpha^2}\right],\quad Q_{12} = Q_{21} = 2G(z)\frac{\lambda_u + M\alpha^2}{2G(z) + \lambda_u + M\alpha^2},$$
$$Q_{44} = Q_{55} = Q_{66} = G(z),\ c_0 = \frac{2G(z)\left[M\alpha^2\left(\beta_f - \beta_s^{"}\right) + 3K_u\beta_s^{'}\right]}{2G(z) + \lambda_u + M\alpha^2} \tag{9}$$

By integrating the stress components along the thickness direction, we obtain the internal force and moment components as follows

$$\begin{aligned}
&N_x = I_{11}\varepsilon_x^0 + I_{12}\varepsilon_y^0 + I_{13}k_x^1 + I_{14}k_y^1 + I_{15}k_x^3 + I_{16}k_y^3 - I_{17}\Phi_1,\\
&N_y = I_{12}\varepsilon_x^0 + I_{11}\varepsilon_y^0 + I_{14}k_x^1 + I_{13}k_y^1 + I_{16}k_x^3 + I_{15}k_y^3 - I_{17}\Phi_1, N_{xy} = I_{31}\gamma_{xy}^0 + I_{32}k_{xy}^1 + I_{33}k_{xy}^3,\\
&M_x = I_{13}\varepsilon_x^0 + I_{14}\varepsilon_y^0 + I_{43}k_x^1 + I_{44}k_y^1 + I_{45}k_x^3 + I_{46}k_y^3 - I_{17}\Phi_2,\\
&M_y = I_{14}\varepsilon_x^0 + I_{13}\varepsilon_y^0 + I_{44}k_x^1 + I_{43}k_y^1 + I_{46}k_x^3 + I_{45}k_y^3 - I_{17}\Phi_2, M_{xy} = I_{32}\gamma_{xy}^0 + I_{62}k_{xy}^1 + I_{63}k_{xy}^3,\\
&P_x = I_{15}\varepsilon_x^0 + I_{16}\varepsilon_y^0 + I_{45}k_x^1 + I_{46}k_y^1 + I_{75}k_x^3 + I_{76}k_y^3 - I_{17}\Phi_4,\\
&P_y = I_{16}\varepsilon_x^0 + I_{15}\varepsilon_y^0 + I_{46}k_x^1 + I_{45}k_y^1 + I_{76}k_x^3 + I_{75}k_y^3 - I_{17}\Phi_4, P_{xy} = I_{33}\gamma_{xy}^0 + I_{63}k_{xy}^1 + I_{93}k_{xy}^3,\\
&P_x = I_{15}\varepsilon_x^0 + I_{16}\varepsilon_y^0 + I_{45}k_x^1 + I_{46}k_y^1 + I_{75}k_x^3 + I_{76}k_y^3 - I_{17}\Phi_4,\\
&P_y = I_{16}\varepsilon_x^0 + I_{15}\varepsilon_y^0 + I_{46}k_x^1 + I_{45}k_y^1 + I_{76}k_x^3 + I_{75}k_y^3 - I_{17}\Phi_4,\\
&P_{xy} = I_{33}\gamma_{xy}^0 + I_{63}k_{xy}^1 + I_{93}k_{xy}^3, Q_x = I_{31}\gamma_{xz}^0 + I_{62}k_{xz}^2,\\
&Q_y = I_{31}\gamma_{yz}^0 + I_{62}k_{yz}^2,\ K_x = I_{62}\gamma_{xz}^0 + I_{63}k_{xz}^2, K_y = I_{62}\gamma_{yz}^0 + I_{63}k_{yz}^2
\end{aligned} \tag{10}$$

where coefficients $I_{ij}\ \left(i, j = 1,2,3,4,5,6,7\right), \Phi_k\ \left(k = 1,2,4\right)$ are expressed in Appendix A.

The motion equations of the saturated porous FG plate are expressed as [12]:

$$\frac{\partial N_x}{\partial x}+\frac{\partial N_{xy}}{\partial y}=I_1\frac{\partial^2 u}{\partial t^2}+\overline{I}_2\frac{\partial^2 \phi_x}{\partial t^2}-\overline{I}_3\frac{\partial^3 w}{\partial t^2\partial x},\frac{\partial N_{xy}}{\partial x}+\frac{\partial N_y}{\partial y}=I_1\frac{\partial^2 v}{\partial t^2}+\overline{I}_2\frac{\partial^2 \phi_y}{\partial t^2}-\overline{I}_3\frac{\partial^3 w}{\partial t^2\partial y},$$

$$\frac{\partial Q_x}{\partial y}+\frac{\partial Q_y}{\partial y}+c_1\left(\frac{\partial^2 P_x}{\partial x^2}+2\frac{\partial^2 P_{xy}}{\partial x\partial y}+\frac{\partial^2 P_y}{\partial y^2}\right)+q+N_x\frac{\partial^2 w}{\partial x^2}+2N_{xy}\frac{\partial^2 w}{\partial x\partial y}+N_y\frac{\partial^2 w}{\partial y^2}-k_1 w+k_2\nabla^2 w$$

$$=I_1\frac{\partial^2 w}{\partial t^2}+2\varepsilon I_1\frac{\partial w}{\partial t}+\overline{I}_3\frac{\partial^3 u}{\partial t^2\partial x}+\overline{I}_5\frac{\partial^3 \phi_x}{\partial t^2\partial x}+\overline{I}_3\frac{\partial^3 v}{\partial t^2\partial y}+\overline{I}_5\frac{\partial^3 \phi_y}{\partial t^2\partial y}-c_1^2 I_7\left(\frac{\partial^4 w}{\partial t^2\partial x^2}+\frac{\partial^4 w}{\partial t^2\partial y^2}\right),$$

$$\frac{\partial M_x}{\partial x}+\frac{\partial M_{xy}}{\partial y}-Q_x-c_1\left(\frac{\partial P_x}{\partial x}+\frac{\partial P_{xy}}{\partial y}\right)=\overline{I}_2\frac{\partial^2 u}{\partial t^2}+\overline{I}_4\frac{\partial^2 \phi_x}{\partial t^2}-\overline{I}_5\frac{\partial^3 w}{\partial t^2\partial x},\tag{11}$$

$$\frac{\partial M_x}{\partial x}+\frac{\partial M_{xy}}{\partial y}-Q_y-c_1\left(\frac{\partial P_{xy}}{\partial x}+\frac{\partial P_y}{\partial y}\right)=\overline{I}_2\frac{\partial^2 v}{\partial t^2}+\overline{I}_4\frac{\partial^2 \phi_y}{\partial t^2}-\overline{I}_5\frac{\partial^3 w}{\partial t^2\partial y}$$

with q is an external pressure uniformly distributed on the surface of the porous plate and

$$\overline{I}_2=I_2-c_1I_4,\overline{I}_3=c_1I_4,\overline{I}_4=I_3-2c_1I_5+c_1^2I_7,\overline{I}_5=c_1I_5-c_1^2I_7,$$
$$\left(I_1,I_2,I_3,I_4,I_5,I_7,\right)=\int_{-h/2}^{h/2}\rho(z)\left(1,z,z^2,z^3,z^4,z^6\right)dz\tag{12}$$

The geometrical compatibility equation is expressed as follows:

$$I_{11}^*\frac{\partial^4 f}{\partial x^4}+I_{11}^*\frac{\partial^4 f}{\partial y^4}+U_1\frac{\partial^4 f}{\partial x^2\partial y^2}+U_2\frac{\partial^3 \phi_x}{\partial x^3}+U_3\frac{\partial^3 \phi_x}{\partial x\partial y^2}+U_4\frac{\partial^3 \phi_y}{\partial y^3}+U_5\frac{\partial^3 \phi_y}{\partial x^2\partial y}-c_1I_{25}^*\frac{\partial^4 w}{\partial x^4}$$
$$-c_1I_{16}^*\frac{\partial^4 w}{\partial y^4}+U_6\frac{\partial^4 w}{\partial x^2\partial y^2}=\left(\frac{\partial^2 w}{\partial x\partial y}\right)^2-\frac{\partial^2 w}{\partial x^2}\frac{\partial^2 w}{\partial y^2}+2\frac{\partial^2 w}{\partial x\partial y}\frac{\partial^2 w^*}{\partial x\partial y}-\frac{\partial^2 w}{\partial x^2}\frac{\partial^2 w^*}{\partial y^2}-\frac{\partial^2 w^*}{\partial x^2}\frac{\partial^2 w}{\partial y^2}\tag{13}$$

where

$$U_1=I_{31}^*-2I_{12}^*,U_2=I_{14}^*-c_1I_{16}^*,U_3=I_{13}^*-c_1I_{15}^*-I_{32}^*+I_{33}^*c_1,U_4=I_{14}^*-c_1I_{16}^*,$$
$$U_5=I_{14}^*-c_1I_{15}^*-I_{32}^*+I_{33}^*c_1,\ U_6=-c_1I_{15}^*-c_1I_{15}^*+2I_{33}^*c_1,\Delta=I_{11}^2-I_{12}^2,I_{11}^*=\frac{I_{11}}{\Delta},I_{12}^*=\frac{I_{12}}{\Delta},$$
$$I_{13}^*=\frac{I_{14}I_{12}-I_{13}I_{11}}{\Delta},\ I_{14}^*=\frac{I_{13}I_{12}-I_{14}I_{11}}{\Delta},I_{15}^*=\frac{I_{16}I_{12}-I_{15}I_{11}}{\Delta},\ I_{16}^*=\frac{I_{15}I_{12}-I_{16}I_{11}}{\Delta},\tag{14}$$
$$I_{17}^*=\frac{I_{11}I_{17}-I_{12}I_{17}}{\Delta},I_{31}^*=\frac{1}{I_{31}},I_{32}^*=-\frac{I_{32}}{I_{31}},I_{33}^*=-\frac{I_{33}}{I_{31}}$$

and the stress function is defined as:

$$N_x=\frac{\partial^2 f}{\partial y^2},\ N_y=\frac{\partial^2 f}{\partial x^2},N_{xy}=-\frac{\partial^2 f}{\partial x\partial y}\tag{15}$$

Substituting Eqs. (4), (10) and (11) into Eq. (11), we have

$$I_{11}^{*}\frac{\partial^4 f}{\partial x^4}+I_{11}^{*}\frac{\partial^4 f}{\partial y^4}+Z_1\frac{\partial^4 f}{\partial x^2\partial y^2}+Z_2\frac{\partial^3\phi_x}{\partial x^3}+Z_3\frac{\partial^3\phi_x}{\partial x\partial y^2}+Z_4\frac{\partial^3\phi_y}{\partial y^3}+Z_5\frac{\partial^3\phi_y}{\partial x^2\partial y}-c_1I_{25}^{*}\frac{\partial^4 w}{\partial x^4}$$
$$-c_1I_{16}^{*}\frac{\partial^4 w}{\partial y^4}+Z_6\frac{\partial^4 w}{\partial x^2\partial y^2}=\left(\frac{\partial^2 w}{\partial x\partial y}\right)^2-\frac{\partial^2 w}{\partial x^2}\frac{\partial^2 w}{\partial y^2}+2\frac{\partial^2 w}{\partial x\partial y}\frac{\partial^2 w^{*}}{\partial x\partial y}-\frac{\partial^2 w}{\partial x^2}\frac{\partial^2 w^{*}}{\partial y^2}-\frac{\partial^2 w^{*}}{\partial x^2}\frac{\partial^2 w}{\partial y^2} \quad (16)$$

where

$$Z_1=I_{31}^{*}-2I_{12}^{*};\ Z_2=I_{14}^{*}-c_1I_{16}^{*};\ Z_3=I_{13}^{*}-c_1I_{15}^{*}-I_{32}^{*}+I_{33}^{*}c_1,$$
$$Z_4=I_{14}^{*}-c_1I_{16}^{*};\ Z_5=I_{14}^{*}-c_1I_{15}^{*}-I_{32}^{*}+I_{33}^{*}c_1;\ Z_6=-c_1I_{15}^{*}-c_1I_{15}^{*}+2I_{33}^{*}c_1 \quad (17)$$

In this paper, we assume that all four edges of the saturated porous FG plate are subjected to simple support conditions. The boundary conditions are

$$\text{At } x=0,\ a:\ w=u=\phi_y=M_x=N_{xy}=0,\ N_x=N_{x0};\ \text{at } y=0,\ b:$$
$$w_0=\theta_x=N_{xy}=M_y=0;N_y=N_{x0} \quad (18)$$

Based on boundary conditions and geometrical compatibility equations, the solutions are assumed to have the following forms:

$$w(x,y,t)=W(t)\sin\lambda_m x\sin\delta_n y,\ w^{*}(x,y,t)=\mu h\sin\lambda_m x\sin\delta_n y$$
$$\phi_x(x,y,t)=\Phi_x(t)\cos\lambda_m x\sin\delta_n y,\phi_y(x,y,t)=\Phi_y(t)\sin\lambda_m x\cos\delta_n y,$$
$$f(x,y,t)=A_1\cos 2\lambda_m x+A_2\cos 2\delta_n y+A_3\sin\lambda_m x\sin\delta_n y+\frac{1}{2}N_{y0}x^2+\frac{1}{2}N_{x0}y^2 \quad (19)$$

in which

$$A_1=\frac{\delta_n^2\left(W^2+2W\mu h\right)}{32I_{11}^{*}\lambda_m^2},A_2=\frac{\lambda_m^2\left(W^2+2W\mu h\right)}{32I_{11}^{*}\delta_n^2},A_3=Q_1W+Q_2\Phi_x+Q_3\Phi_y,$$
$$Q_1=\frac{c_1I_{16}^{*}\lambda_m^4+c_1I_{16}^{*}\delta_n^4-U_6\lambda_m^2\delta_n^2}{I_{11}^{*}\lambda_m^4+I_{11}^{*}\delta_n^4+U_1\lambda_m^2\delta_n^2},Q_2=\frac{-U_2\lambda_m^3-U_3\delta_n^2\lambda_m}{I_{11}^{*}\lambda_m^4+I_{11}^{*}\delta_n^4+U_1\lambda_m^2\delta_n^2},Q_3=\frac{-U_4\delta_n^3-U_5\delta_n\lambda_m^2}{I_{11}^{*}\lambda_m^4+I_{11}^{*}\delta_n^4+U_1\lambda_m^2\delta_n^2} \quad (20)$$

with $\lambda_m=m\pi/a,\ \delta_n=n\pi/b;\ \mu$ is imperfection parameter and W,Φ_x,Φ_y are time dependent amplitudes.

Introducing Eq. (19) into Eq. (16), we have the system of basic differential equations as

$$d_{11}W+d_{12}\Phi_x+d_{13}\Phi_y+r_1\left(W+\mu h\right)\Phi_x+r_2\left(W+\mu h\right)\Phi_y+r_3\left(W+\mu h\right)+r_4W\left(W+\mu h\right)$$
$$+n_3W\left(W+2\mu h\right)+r_5W\left(W+\mu h\right)\left(W+2\mu h\right)+n_5q=I_0\frac{d^2W}{dt^2}+2\varepsilon I_1\frac{dW}{dt}-\lambda_m\overline{\overline{I}}_5\frac{d^2\Phi_x}{dt^2}-\delta_n\overline{\overline{I}}_5\frac{d^2\Phi_y}{dt^2},$$
$$d_{21}W+d_{22}\Phi_x+d_{23}\Phi_y+n_6\left(W+\mu h\right)+n_7W\left(W+\mu h\right)=\overline{\overline{I}}_3\frac{d^2\Phi_x}{dt^2}-\lambda_m\overline{\overline{I}}_5\frac{d^2W}{dt^2},$$
$$d_{31}W+d_{32}\Phi_x+d_{33}\Phi_y+n_8\left(\mathrm{W}+\mu h\right)+n_9W\left(W+\mu h\right)=\overline{\overline{I}}_3\frac{d^2\Phi_y}{dt^2}-\delta_n\overline{\overline{I}}_5\frac{d^2W}{dt^2} \quad (21)$$

where

$$r_1=l_{14}-m_2\lambda_m^2-m_2^{*}\delta_n^2,r_2=l_{15}-m_3\lambda_m^2-m_3^{*}\delta_n^2,r_3=n_1-2m_4\Phi_1\left(\lambda_m^2+\delta_n^2\right),\ r_4=n_2-m_1\lambda_m^2-m_1^{*}\delta_n^2,$$
$$r_5=n_4-m_5\lambda_m^2-m_5^{*}\delta_n^2,\overline{\overline{I}}_3=\overline{I}_4-\frac{\left(\overline{I}_2\right)^2}{I_1},\overline{\overline{I}}_5=\overline{I}_5-\frac{\overline{I}_3\overline{I}_2}{I_1},\overline{\overline{I}}_7=\frac{\left(\overline{I}_3\right)^2}{I_1}-c_1^2I_7. \quad (22)$$

and the coefficients $d_{ij}\ (i,j=1,2,3,4), n_k\ \left(k=\overline{1,9}\right)$ are given in Appendix B.

The natural frequency of the saturated porous FG plate is obtained by following equation:

$$\begin{vmatrix} l_{11}+r_3+I_0\omega^2 & l_{12}-\lambda_m\overline{\overline{I}}_5\omega^2 & l_{13}-\delta_n\overline{\overline{I}}_5\omega^2 \\ l_{21}+n_6-\lambda_m\overline{\overline{I}}_5\omega^2 & l_{22}+\overline{\overline{I}}_3\omega^2 & l_{23} \\ l_{31}+n_8-\delta_n\overline{\overline{I}}_5\omega^2 & l_{32} & l_{33}+\overline{\overline{I}}_3\omega^2 \end{vmatrix}=0 \tag{23}$$

Using the harmonic balance method, the frequency ratio – amplitude relation of free vibration is as follows:

$$\omega_{NL}=\omega_L\left(1+\frac{8}{3\pi}N\xi+\frac{3P}{4}\xi^2\right)^{1/2} \tag{24}$$

with

$$N=\frac{\left(a_3+a_4+a_6\right)}{\left(a_1+a_2\right)}, P=\frac{\left(a_5+a_7\right)}{\left(a_1+a_2\right)}, a_1=l_{11}+l_{12}g_{12}+g_{23}g_{22}, a_2=l_{12}g_{13}+l_{13}g_{23}+r_3, a_3=l_{12}g_{14}+l_{13}g_{24} \tag{25}$$

$$+r_1g_{12}+r_2g_{22}+r_4, a_4=r_1g_{13}+r_2g_{23}, a_5=r_1g_{14}+r_2g_{24}, a_6=n_3, a_7=r_5, a_8=n_5, a_9=I_0-l_{12}g_{11}-l_{13}g_{21}$$

and the coefficients $g_{ij}\ (i=1,2;\ j=\overline{1,4})$ are expressed in Appendix C.

4. Results and Discussion

To verify the precision and dependability of our current approach, we calculated the dimensionless frequency $\lambda=\omega\left(b/\pi\right)^2\sqrt{\rho h/D}$ with $D=Eh^3/\left[12\left(1-\nu^2\right)\right]$ of the porous isotropic plate and compared it against the numerical findings of Xue et al., [11], which were derived from a higher order shear deformation theory. The data in Table 1 show a strong alignment between the obtained results and those of Xue et al., [11], showcasing a maximum discrepancy of just 1.12%. This outcome solidifies the credibility of our method.

Table 1. Comparison of the dimensionless frequency of the porous isotropic plate

Porosity distribution types	Source	e_0			
		0.2	0.3	0.4	0.5
Symmetric distribution	Present	1.9372	1.9051	1.9283	1.9334
	Xue et al., [11]	1.9228	1.9210	1.9220	1.9269
	Error	0.74%	0.82%	0.32%	0.33%
Asymmetric distribution	Present	1.8962	1.8459	1.8142	1.7456
	Xue et al., [11]	1.8754	1.8424	1.8050	1.7612
	Error	1.12%	0.19%	0,5%	0.88%
Evenly distribution	Present	1.8541	1.8222	1.7858	1.7439
	Xue et al., [11]	1.8656	1.8285	1.7877	1.7423
	Error	0.61%	0.34%	0.1%	0.1%

Table 2 illustrates the influences of elastic foundation coefficients, temperature increment and b/h ratio on the natural frequency (rad/s) of a saturated porous FG plate. Three values of the temperature increment, three values of the b/h ratio and five values of the elastic foundation coefficients are considered. Evidently, as the moduli of the elastic foundation, $k_1\,(GPa/m)$ and $k_2\,(GPa.m)$, increase, the natural frequency of the saturated porous FG plate also increases. This phenomenon can be attributed to the positive support provided by the elastic foundations, which enhances the structural stiffness of the plate and consequently raises the natural frequency. Conversely, an increase in both the temperature increment and b/h ratio results in reduced plate stiffness, leading to a corresponding decrease in the natural frequency.

Table 2. Effects of the elastic foundation coefficients, temperature increment and b/h ratio on the natural frequency of a saturated porous FG plate

$\Delta T(K)$	b/h	(k_1,k_2)				
		$(0.1,0.05)$	$(0.15,0.05)$	$(0.2,0.05)$	$(0.2,0.08)$	$(0.2,0.1)$
0	10	5780.974	5791.340	5801.687	6273.643	6569.546
	15	3060.003	3079.781	3099.467	3487.629	3723.979
	20	2051.418	2080.837	2109.992	2428.081	2618.748
200	10	5374.343	5385.523	5396.758	5901.193	6214.765
	15	2707.146	2729.516	2751.640	3182.542	3439.923
	20	1749.178	1783.691	1817.519	2178.717	2389.383
400	10	4934.340	4946.607	4958.720	5503.450	5838.424
	15	2300.834	2327.086	2353.026	2844.926	3130.223
	20	1382.365	1425.786	1467.882	1896.873	2135.505

Table 3. Effects of the b/a ratio, pore coefficient e_0 and Skempton coefficient B on the natural frequency of a saturated porous FG plate

b/a	B	e_0		
		0.1	0.4	0.7
0.5	0.2	6449.601	5925.496	5206.558
	0.5	6466.146	5985.421	5298.264
	0.8	6482.202	6043.125	5380.609
1	0.2	2921.195	2764.069	2531.435
	0.5	2925.302	2782.213	2562.431
	0.8	2929.316	2799.299	2590.476
1.5	0.2	2248.428	2157.162	2011.069
	0.5	2250.375	2167.814	2031.348
	0.8	2252.280	2177.878	2049.758

Table 3 indicates the effects of the b/a ratio, pore coefficient e_0 and Skempton coefficient B on the natural frequency of a saturated porous FG plate. The findings indicate a substantial decrease in the natural frequency of the plate when either the porous coefficient or the b/a ratio is increased. This

phenomenon can be explained by the concurrent reduction in the stiffness of the plate and elastic modulus resulting from these increases. Conversely, a slight increase in the natural frequency of the plate is observed with the augmentation of the Skempton coefficient.

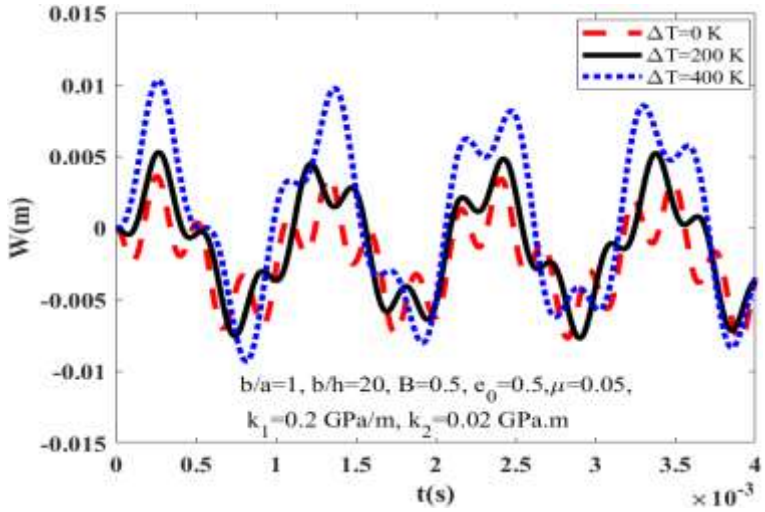

Figure 2. Effect of temperature change of graphene on the deflection amplitude – time relation of the saturated porous FG plate.

Figures 3 and 4 illustrate the effects of porosity coefficient on the relationship between deflection amplitude and time as well as frequency ratio and amplitude, respectively. The temperature change is $\Delta T = 200\,K$ and the Skempton coefficient is $B = 0.5$. As previously noted, the structural stiffness of the saturated porous FG plate diminishes as the porosity coefficient value rises. Consequently, elevating the porosity coefficient value will lead to an augmentation in both the plate's deflection amplitude and frequency ratio.

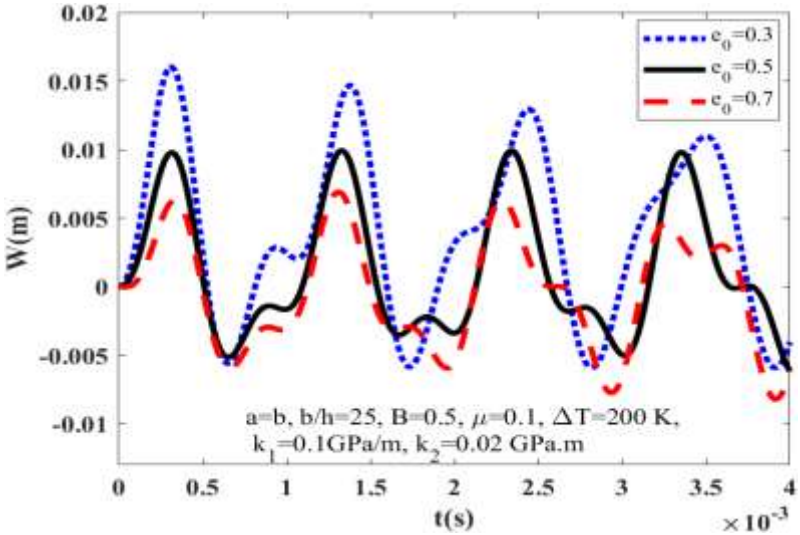

Figure 3. Effect of porosity coefficient on the on the deflection amplitude – time relation of the saturated porous FG plate.

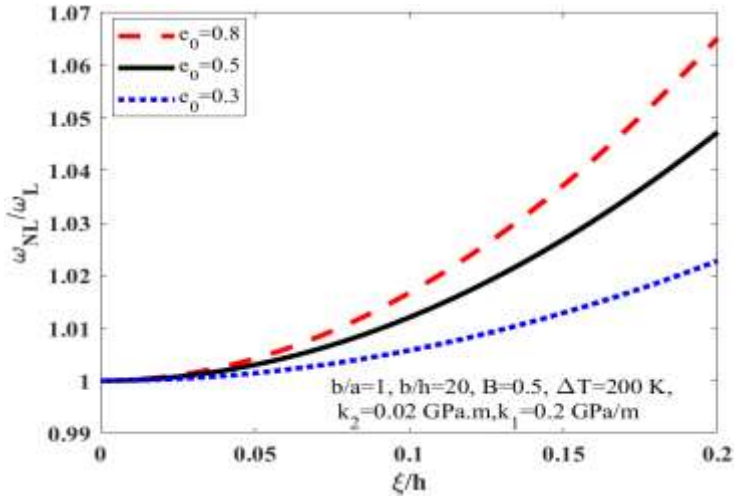

Figure 4. Effect of porosity coefficient on the on the frequency ratio – amplitude of the saturated porous FG plate.

Figure 5 presents the influence of Skempton coefficient on the on the frequency ratio – amplitude of the saturated porous FG plate subjected to the combination of mechanical and thermal loadings. Three Skempton coefficient values $B = 0.2, 0.5$ and 0.8 are under examination. It becomes evident that as the Skempton coefficient rises, the pressure of water or gas within the pores increases, resulting in a reduction in the frequency ratio when considered alongside the amplitude of the vibration.

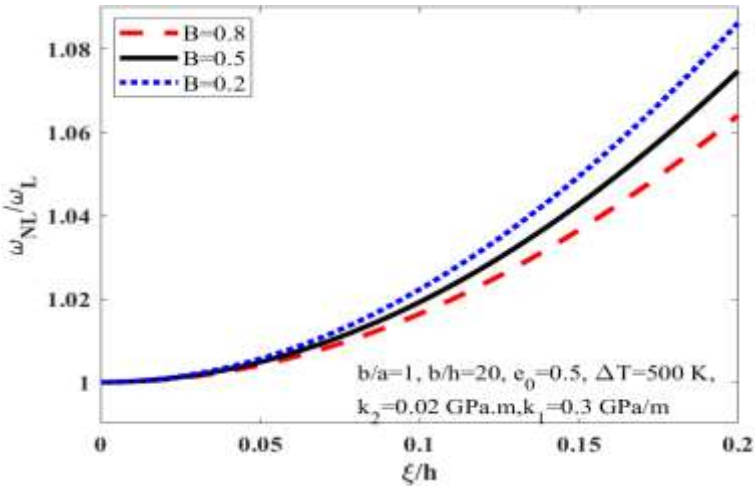

Figure 5. Effect of Skempton coefficient on the on the frequency ratio – amplitude of the saturated porous FG plate.

Figure 6 shows the frequency ratio – amplitude of the saturated porous FG plate in thermal environment with three different types of porosity distribution. The porosity coefficient is taken to be $e_0 = 0.5$. Clearly, when the amplitude is held constant, the saturated porous plate with porosity monotonous distribution type will exhibit the highest frequency ratio value, while porosity nonsymmetric distribution type will show the lowest frequency ratio.

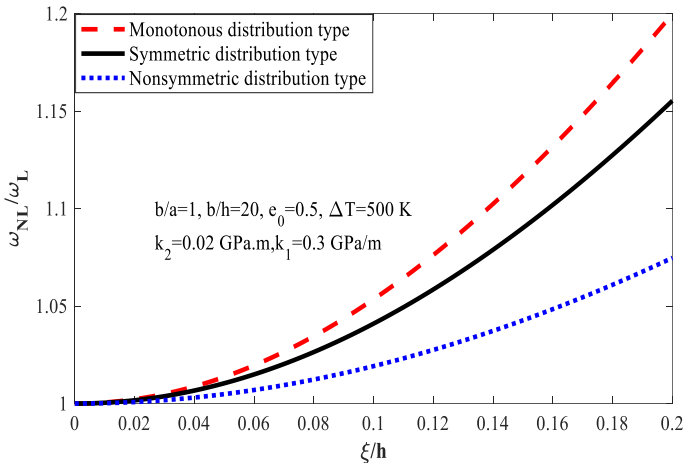

Figure 6. Effect of three different porosity distribution types on the on the frequency ratio – amplitude of the saturated porous FG plate.

5. Conclusions

In summary, in this work we investigated the nonlinear vibration characteristics of an imperfect saturated porous FG plate on elastic foundations. The set of nonlinear differential equations for this system are derived using the Biot theory and Hamilton's principle. Several noteworthy insights emerge from the numerical findings:

- The increase in the porosity coefficient leads to a decrease in the natural frequency while simultaneously causing an increase in both deflection amplitude and the frequency ratio of the saturated porous plate.

- Although the Skempton coefficient exerts a relatively minor influence, it positively affects the stiffness of the saturated porous plate. Consequently, an increase in the Skempton coefficient raises the natural frequency and reduces the frequency ratio of the saturated porous plate.

- The presence of elastic foundations providing support to the porous plate during load-bearing operations enhances the values of its natural frequency through this supportive mechanism.

- As the temperature change is increased, the natural frequency of the porous plate experiences a significant reduction, while the deflection amplitude shows an increase. This phenomenon can be attributed to the adverse impact of temperature on the stiffness and elastic modulus of the saturated porous plate.

- Porosity monotonous distribution type will result in the saturated porous plate having the highest frequency ratio value, while porosity nonsymmetric distribution type will lead to the lowest frequency ratio.

- The nonlinear vibration characteristics of the porous plate are significantly influenced by geometric parameters.

Acknowledgments

This work was financially supported by VNU University of Engineering and Technology under project number CN23.05.

References

[1] Y. Xue, G. Jin, C. Zhang, X. Han, J. Chen, Free Vibration Analysis of Functionally Graded Porous Cylindrical Panels and Shells with Porosity Distributions along The Thickness and Length Directions, Thin-Walled Structures, Vol. 184, 2023, pp. 110448, https://doi.org/10.1016/j.tws.2022.110448.

[2] H. Chaabani, S. Mesmoudi, L. Boutahar, K. E. Bikri, A High-order Finite Element Continuation for Buckling Analysis of Porous FGM Plates, Engineering Structures, Vol. 279, 2023, pp. 115597, https://doi.org/10.1016/j.engstruct.2023.115597.

[3] Q. He, Y. L. Zhou, M. Li, L. He, H. L. Dai, Nonlinear Vibration Analysis of CFRR Sandwich Doubly-Curved Shallow Shells with A Porous Microcapsule Coating in Hygrothermal Environment, Thin-Walled Structures, Vol. 185, 2023, pp. 115597, https://doi.org/10.1016/j.tws.2023.110587.

[4] Y. Yang, T. Dai, H. L. Dai, Hygro-thermo-mechanical Coupling Behavior of Porous FG-GNPRC Annular Plates Considering Aggregation of GNPs, Thin-Walled Structures, Vol. 192, 2023, pp. 111145, https://doi.org/10.1016/j.tws.2023.111145.

[5] N. T. Do, T. T. Tran, T. N. Thoi, Q. H. Pham, An Improved MITC3 Element for Vibration Response Analysis of Piezoelectric Functionally Graded Porous Plates, Forces in Mechanics, Vol. 13, 2023, pp. 100231, https://doi.org/10.1016/j.finmec.2023.100231.

[6] Ö. Civalek, B. Uzun, M. Ö. Yaylı, On Nonlinear Stability Analysis of Saturated Embedded Porous Nanobeams, International Journal of Engineering Science, Vol. 190, 2023, pp. 103898, https://doi.org/10.1016/j.ijengsci.2023.103898.

[7] W. H. Yuan, J. X. Zhu, K. Liu, W. Zhang, B. B. Dai, Y. Wang, Dynamic Analysis of Large Deformation Problems in Saturated Porous Media by Smoothed Particle Finite Element Method, Computer Methods in Applied Mechanics and Engineering, Vol. 392, 2022, pp. 114724, https://doi.org/10.1016/j.cma.2022.114724.

[8] Y. Zhao, X. Chen, Z. Chen, D. Ling, Z. Shan, Y. Wang, A Semi-analytical Solution for The Transient Response of One-dimensional Saturated Single-layer Porous Media with General Boundary Conditions, Transportation Geotechnics, Vol. 42, 2023, pp. 101006, https://doi.org/10.1016/j.trgeo.2023.101006.

[9] M. Babaei, K. Asemi, F. Kiarasi, Dynamic Analysis of Functionally Graded Rotating Thick Truncated Cone Made of Saturated Porous Materials, Thin-Walled Structures, Vol. 164, 2021, pp. 107852, https://doi.org/10.1016/j.tws.2021.107852.

[10] Z. Ba, J. Niu, Y. Liu, J. Liang, Dynamic Response of A Multi-scale Layered Saturated Porous Half-space Due to Seismic Dislocation Source by Using A Revised Dynamic Stiffness Matrix Method, Applied Mathematical Modelling, Vol. 120, 2023, pp. 217-245, https://doi.org/10.1016/j.apm.2023.03.033.

[11] Y. Xue, G. Jin, X. Ma, H. Chen, T. Ye, M. Chen et al., Free Vibration Analysis of Porous Plates with Porosity Distributions in The Thickness and In-plane Directions Using Isogeometric Approach, International Journal of Mechanical Science, Vol. 152, 2019, pp. 346-362, https://doi.org/10.1016/j.ijmecsci.2019.01.004.

[12] J. N. Reddy, Mechanics of Laminated Composite Plates and Shells: Theory and Analysis. Boca Raton: CRC Press, 2004.

[13] M. A. Biot, Theory of Buckling of A Porous Slab and Its Thermoelastic Analogy, Journal of Applied Mechanics, Vol. 31, No. 2, 1964, pp. 194-198, https://doi.org/10.1115/1.3629586.

Appendixes

Appendix A

$$I_{11}=\int_{-h/2}^{h/2}Q_{11}dz, I_{12}=\int_{-h/2}^{h/2}Q_{12}dz, I_{13}=\int_{-h/2}^{h/2}Q_{11}zdz; I_{14}=\int_{-h/2}^{h/2}Q_{12}zdz, I_{15}=\int_{-h/2}^{h/2}Q_{11}z^3dz, I_{16}=\int_{-h/2}^{h/2}Q_{12}z^3dz,$$

$$I_{17}=1;\left(\Phi_1,\Phi_2,\Phi_4\right)=\int_{-h/2}^{h/2}c_0\left(z\right)T\left(1,z,z^3\right)dz, I_{31}=\int_{-h/2}^{h/2}Q_{66}dz, I_{32}=\int_{-h/2}^{h/2}Q_{66}zdz, I_{33}=\int_{-h/2}^{h/2}Q_{66}z^3dz,$$

$$I_{43}=\int_{-h/2}^{h/2}Q_{11}z^2dz, I_{44}=\int_{-h/2}^{h/2}Q_{12}z^2dz; I_{45}=\int_{-h/2}^{h/2}Q_{11}z^4dz; I_{46}=\int_{-h/2}^{h/2}Q_{12}z^4dz, I_{62}=\int_{-h/2}^{h/2}Q_{66}z^2dz,$$

$$I_{63}=\int_{-h/2}^{h/2}Q_{66}z^4dz, I_{75}=\int_{-h/2}^{h/2}Q_{11}z^6dz, I_{76}=\int_{-h/2}^{h/2}Q_{12}z^6dz, I_{93}=\int_{-h/2}^{h/2}Q_{66}z^6dz$$

Appendix B

$$d_{11}=D_{12}\lambda_m^4+D_{13}\lambda_m^2\delta_n^2+D_{14}\delta_n^4-k_1-k_2\left(\lambda_m^2+\delta_n^2\right)+Q_1\left(D_{19}\lambda_m{}^4+D_{110}\lambda_m^2\delta_n^2+D_{111}\delta_n^4\right),$$

$$d_{12}=-D_{11}\lambda_m+D_{15}\lambda_m^3+D_{16}\lambda_m\delta_n^2+Q_2\left(D_{19}\lambda_m{}^4+D_{110}\lambda_m^2\delta_n^2+D_{111}\delta_n^4\right),$$

$$d_{13}=-D_{11}\delta_n+D_{17}\delta_n^3+D_{18}\lambda_m^2\delta_n+Q_3\left(D_{19}\lambda_m{}^4+D_{110}\lambda_m^2\delta_n^2+D_{111}\delta_n^4\right),$$

$$d_{14}=-\frac{32}{3mn\pi^2}\lambda_m^2\delta_n^2Q_2, d_{15}=-\frac{32}{3mn\pi^2}\lambda_m^2\delta_n^2Q_3, n_1=-D_{11}\lambda_m^2-D_{11}\delta_n^2, n_2=-\frac{32}{3mn\pi^2}\lambda_m^2\delta_n^2Q_1,$$

$$n_3=-\frac{\lambda_m^2\delta_n^2\left(D_{19}+D_{111}\right)}{4I_{11}^*}, n_4=-\frac{\lambda_m^4+\delta_n^4}{16I_{11}^*}, n_5=\frac{16}{mn\pi^2}, I_0=I_1-\overline{\overline{I_7}}\left(\lambda_m^2+\delta_n^2\right),$$

$$d_{21}=-D_{22}\lambda_m^3-D_{23}\lambda_m\delta_n^2-D_{27}\lambda_m^3Q_1-D_{28}\lambda_m\delta_n^2Q_1, d_{22}=D_{21}-D_{24}\lambda_m^2-D_{25}\delta_n^2-D_{27}\lambda_m^3Q_2-D_{28}\lambda_m\delta_n^2Q_2,$$

$$d_{23}=-D_{26}\lambda_m\delta_n-D_{27}\lambda_m^3Q_3-D_{28}\lambda_m\delta_n^2Q_3, n_6=D_{21}\lambda_m, n_7=-\frac{4D_{27}\lambda_m\delta_n^2}{3I_{11}^*mn\pi^2},$$

$$d_{31}=-D_{32}\delta_n^3-D_{33}\lambda_m^2\delta_n-D_{38}\lambda_m^2\delta_nQ_1-D_{37}\delta_n^3Q_1, d_{32}=-D_{34}\lambda_m\delta_n-D_{38}\lambda_m\delta_n^2Q_2-D_{37}\delta_n^3Q_2,$$

$$d_{33}=D_{21}-D_{35}\lambda_m^2-D_{36}\delta_n^2-D_{38}\lambda_m\delta_n^2Q_3-D_{37}\delta_n^3Q_3, n_8=D_{21}\delta_n, n_9=-\frac{4D_{37}\lambda_m^2\delta_n}{3I_{11}^*mn\pi^2}.$$

Appendix C

$$g_{11}=\frac{\overline{\overline{I_5}}\left(-\overline{\overline{I_5}}\lambda_m l_{33}+\overline{\overline{I_5}}\delta_n l_{23}\right)}{\left(l_{33}l_{22}-l_{23}l_{32}\right)}, g_{12}=\frac{\left(-l_{21}l_{33}+l_{31}l_{23}\right)}{\left(l_{33}l_{22}-l_{23}l_{32}\right)}, g_{13}=\frac{\left(-n_6l_{33}+n_8l_{23}\right)}{\left(l_{33}l_{22}-l_{23}l_{32}\right)}, g_{14}=\frac{\left(-n_7l_{33}+n_9l_{23}\right)}{\left(l_{33}l_{22}-l_{23}l_{32}\right)},$$

$$g_{21}=\frac{\overline{\overline{I_5}}\left(-\overline{\overline{I_5}}\lambda_m l_{32}+\overline{\overline{I_5}}\delta_n l_{22}\right)}{\left(l_{32}l_{23}-l_{33}l_{22}\right)}, g_{22}=\frac{\left(-l_{21}l_{32}+l_{31}l_{22}\right)}{\left(l_{32}l_{23}-l_{33}l_{22}\right)}, g_{23}=\frac{\left(-n_6l_{32}+n_8l_{22}\right)}{\left(l_{32}l_{23}-l_{33}l_{22}\right)}, g_{34}=\frac{\left(-n_7l_{32}+n_9l_{22}\right)}{\left(l_{32}l_{23}-l_{33}l_{22}\right)}$$